ARTICLES

First-principles theory of Ta up to 10 Mbar pressure: Structural and mechanical properties

Per Söderlind and John A. Moriarty

Physics and Space Technology Directorate, Lawrence Livermore National Laboratory, University of California, P.O. Box 808,
Livermore, California 94551

Fundamental high-pressure structural and mechanical properties of Ta have been investigated theoretically over a wide pressure range, $0-10$ Mbar, by means of *ab initio* electronic-structure calculations. The calculations are fully relativistic and use a state-of-the-art treatment of gradient corrections to the exchange-correlation potential and energy within density-functional theory. The calculated zero-temperature equation of state for bcc Ta is in good agreement with diamond-anvil-cell measurements up to 750 kbar and with reduced shock data to 2.3 Mbar. The crystal-structure stability among bcc, fcc, hcp, and $A15$ phases has been studied as a function of compression and the observed ambient-pressure bcc phase is found to be thermodynamically stable throughout the entire $0-10$ Mbar range. At the upper end of this range, a metastable fcc phase develops with positive elastic moduli and a decreasing fcc$-$bcc energy difference, suggesting that at even higher pressures above 10 Mbar, fcc Ta will become stable over the bcc phase. Elastic constants, the H- and N-point zone-boundary phonons, and the ideal shear strength have also been calculated for bcc Ta up to 10 Mbar pressure. The elastic moduli and phonons are in good agreement with experiment at ambient pressure and remain real and positive for all compressions studied, demonstrating that the bcc phase is mechanically stable in this regime. The calculated elastic constants validate the assumed pressure scaling of the shear modulus in the Steinberg-Guinan strength model of Ta, while the calculated values of ideal shear strength provide an upper bound to the high-pressure yield stress. [S0163-1829(98)01117-5]

I. INTRODUCTION

The thermodynamic and mechanical properties of tantalum (Ta) have been of long standing scientific and applications interest in both the high-pressure and materials physics communities. From the high-pressure community, a large amount of experimental equation-of-state data exist on this metal, including shock Hugoniot data up to 10 Mbar[1–3] and static compression data in the diamond-anvil cell to 750 kbar.[4,5] From the materials community, there is a corresponding wealth of data on the mechanical properties of Ta at or near ambient pressure, including, for example, extensive static test data on the temperature and strain-rate dependence of the yield stress in Ta polycrystals[6] and detailed studies of the plastic deformation behavior of single-crystal bcc metals including Ta.[7] In addition, there have been ultrasonic measurements of the ambient-pressure elastic moduli and their pressure derivatives in Ta and other bcc metals[8] and dynamic mechanical test data on Ta to pressures as high as 2.3 Mbar.[9] These data have been used to construct phenomenological constitutive models of strength in Ta and other metals for high-pressure applications.[9,10]

Theoretically, there has not been heretofore a large corresponding effort to study the fundamental properties of Ta, especially those at high pressure. Although Ta is a prototype bcc transition metal, its 5d relativistic character make its quantitative behavior somewhat more challenging for *ab initio* theory. Moreover, rigorous approaches to treat mechanical properties in metals have generally lagged behind those

of thermodynamic properties. This reflects the fact that mechanical properties depend on phenomena at multiple length scales ranging from atomistic to continuum, whereas thermodynamic properties are determined primarily at the atomistic level and can be directly addressed with quantum-mechanical methods. Recently, however, with the rapid and continuing development of large scale computing capabilities, there has been a growing interest in attempting to bridge the length scales and address mechanical properties from a fundamental perspective as well.[11] At the same time, advances in diamond-anvil-cell research hold promise that both the elastic moduli[12,13] and yield strength[14,15] in metals can be directly measured at megabar pressures. Both of these factors have helped renew interest in studying the mechanical properties of Ta at high pressure.

The purpose of this paper is to present a comprehensive first-principles study of the structural, elastic, vibrational, and ideal-strength properties of bcc Ta in the $0-10$ Mbar pressure range at zero temperature. These fundamental properties not only under pin the high-pressure thermodynamic and mechanical behavior of the metal as a whole but, in addition, they can be used to constrain and validate corresponding interatomic potentials that can directly extend the range of applications to include finite-temperature equation-of-state properties and the treatment of extended defects such as screw dislocations, which control plasticity and other mechanical properties in bcc metals. Our approach is based on an *ab initio*, fully relativistic treatment of the electronic structure of the metal and uses a state-of-the-art implemen-

tation of density-functional theory[16,17] including gradient corrections to the exchange and correlation potential and energy. Within this framework, the equilibrium volume of the metal is calculated to about 1% accuracy and the corresponding equation of state is also shown to be in good agreement with experiment, as are the ambient-pressure elastic moduli and zone-boundary phonon frequencies. We further demonstrate that the observed ambient-pressure bcc phase remains both thermodynamically and mechanically stable over the entire 10 Mbar range considered, and that a metastable fcc phase appears at the upper end of this range and will possibly become lower in energy than bcc at still higher pressures. The calculated high-pressure behavior of the elastic moduli is used to estimate the expected pressure dependence of the shear modulus G in polycrystalline Ta and thereby to test the assumed pressure dependence in the phenomenological Steinberg-Guinan strength model,[10] which scales the yield stress with G. As an upper bound to the high-pressure yield stress, we also consider the pressure dependence of the ideal shear strength of the metal, defined as the minimum stress required to shear the perfect bcc crystal into itself for the observed twinning geometry.

The outline of the paper is as follows. In Sec. II we give a brief overview of the computational approach used in our *ab initio* electronic-structure calculations. Then in Sec. III we discuss the low-temperature equation of state of Ta, while in Sec. IV we investigate the high-pressure structural phase stability of the metal. The pressure dependence of the bcc elastic constants and zone-boundary phonons is considered in Sec. V. Then in Sec. VI we use the calculated elastic constants to analyze the assumed pressure dependence of the Steinberg-Guinan strength model as applied to Ta and we also consider the corresponding ideal shear strength of bcc Ta. Concluding remarks are given in Sec. VII.

II. COMPUTATIONAL APPROACH

The following section briefly summarizes the details of our *ab initio* electronic-structure calculations. Our computational method is based on the first-principles density-functional theory[16,17] and yields the total energy of a periodic system without any experimental input other than the atomic number (73 for Ta). In principle, this theory only involves one approximation, namely, the assumed form of the density functional for the exchange and correlation energy of the electrons. Historically, this functional has usually been treated within the local-density approximation[17] (LDA), but here we have chosen to use what we believe is the most accurate treatment available to date, namely, the generalized gradient approximation (GGA) of Perdew *et al.*[18] In practice, other approximations are often also used in conjunction with any actual computational method. In the present work, we have made a special effort to remove such additional approximations. In particular, (i) the electron charge density and the one-electron potential are allowed to have any geometrical shape and are calculated self-consistently; (ii) all relativistic terms, including the spin-orbit coupling, are included in the Hamiltonian; and (iii) the numerical basis set used is extended to a so-called ''double basis'' set in order to minimize truncation errors in the expansion of the one-electron wave functions. The importance of the GGA

exchange-correlation treatment, the shape-independent electron density and potential, and the spin-orbit coupling have been studied in detail for Ta in the context of the predicted equilibrium volume and zero-temperature equation of state, as will be discussed below in Sec. III.

The present method incorporates nonsphericity to the charge density and potential by representing the crystal with nonoverlapping spheres (of a variable, optimum size) surrounding each atomic site and a general shaped interstitial region between the spheres. Hence, we deal with two types of geometrical regions in the calculations. Inside the spheres, the wave functions are represented as Bloch sums of so-called linear muffin-tin orbitals and are expanded by means of structure constants. The kinetic energy is not restricted to be zero in the interstitial region and the wave function expansion contains Hankel and Neumann functions (depending on sign of the kinetic energy) together with Bessel functions. The analytical expressions for these expansions can be found elsewhere.[19] The whole approach is usually called a full-potential linear muffin-tin orbital (FP-LMTO) method, because of the use of linear muffin-tin orbitals in the wave function expansions and the fact that the potential contains no shape approximation. In order to represent the wave functions in Ta as accurately as possible we have defined here, in a single energy panel, $5s$, $5p$, and $4f$ semi-core states and $6s$, $6p$, $5d$, and $5f$ valence states. The aforementioned ''double basis set'' has been used, i.e., two kinetic energy parameters (κ^2) appropriate for the tails of the $5s$, $5p$, and $4f$ states, and the valence states have been used. Because of the spin-orbit interaction, our calculations involve diagonalizing matrices with dimension 108 per atom.

With such an electronic-structure method that accurately calculates the total energy of a periodic system, it is reasonably straightforward to compute the zero-temperature equation of state, crystal structure stabilities, elastic constants, and high-symmetry zone-boundary phonons, although calculation of the elastic constants and phonons is computationally rather intensive. The approach that has been followed here for these computations is similar to that used recently for a study of iron up to megabar pressures[20] and we therefore make only a few selected comments here and refer the interested reader to that publication for additional details. The calculation of the ideal shear strength, on the other hand, is new in the present context and we discuss its calculation separately in Sec. VI. Except as indicated, all calculations presented here have been performed with the same extended (double) basis set described above, the same (GGA) exchange-correlation functional, and the same fully relativistic treatment with the spin-orbit coupling included.

In obtaining the equation of state for bcc Ta, total energies have been calculated for 21 volumes (corresponding to steps smaller than 1 Å^3). As was discussed previously for iron,[20] the total energy converges slowly with respect to the k-point sampling used in the appropriate summations over the Brillouin zone (BZ) at high pressures. Here we have used up to 150 k points in the irreducible (1/48th) part of the BZ. The 21 total energy points were then locally fit in a least-squares manner using the Murnaghan equation-of-state form.[21] Specifically, the energy-volume data were divided into overlapping sets containing five energy-volume points each for which the four variational parameters of the Mur-

naghan form were individually fitted. In the interior of the data interval, the parameters so determined were then used to calculate the pressure and bulk modulus at the middle of each five-point set. This procedure was modified for the high-end and low-end boundary points where instead the closest five points inside the data interval were used. Hence, a total of 17 fits with 4 variational parameters each were done. For the boundary points the described procedure is of course not as accurate as for the other points. At the high-volume end this was not a problem since we could calculate some energy points well above the equilibrium volume and use these as boundary points. At the high-pressure end this procedure could potentially introduce small errors due to the fitting. However, at high pressure this ''local-fit'' scheme is expected to give similar results to those obtained from a global fit (one Murnaghan fit for all 21 points), and this is in fact the case here. The root-mean-square (rms) errors for the ''global'' and ''local'' fits are about 0.1 mRy and 5 μRy, respectively.

The structural energies for the bcc, fcc, hcp, and the $A15$ (8 atoms per unit cell) phases of Ta have been calculated up to 10 Mbar. In our theoretical treatment, volume, and not pressure, is the independent variable for the total-energy calculations. In principle, the Gibbs free energy as a function of pressure for the two phases in a phase transition should be considered. However, the volume change at a metallic solid-solid phase transition ΔV is usually small ($\sim$ 1 %), and the difference between Gibbs free-energy differences at constant pressure and total-energy differences a constant volume is on the order of $(\Delta V)^2$ and typically negligible.[22] Hence we consider only total-energy differences and calculate the pressure through the bcc Ta EOS. This approximation is not important because the bcc phase remains lower in energy than any of the other phases studied throughout the entire pressure range. Again, care was taken in converging each total-energy result with respect to the number of k points. We have used 150 (bcc), 150 (fcc), 162 (hcp), and 45 ($A15$) k points in the respective irreducible BZ of the four structures considered.

The calculation of the bcc shear elastic constants, C' and C_{44}, has been done in a manner similar to that for iron[20] and as in that case, convergence of the total energies required a large number of k points (2176 and 1620, respectively). The calculation of zone-boundary phonons for bcc Ta was also similar except that a bcc structure has not been previously considered in this context and we therefore mention a few details here and in Appendix A. The bcc phonons have been obtained using the frozen-phonon method,[23] in which the total energy is calculated as a function of static displacements of the atoms corresponding to the phonon under consideration. From the shift in total energy ΔE induced by a small atomic displacement, the angular phonon frequency ($\omega_{\mathbf{q}}$) can be calculated using the relation

$$\Delta E = \frac{1}{2} M (u_{\mathbf{q}} \omega_{\mathbf{q}})^2, \tag{1}$$

where M is the atomic mass for Ta and $u_{\mathbf{q}}$ is the amplitude of the displacement. In this study we only have considered phonons at two high-symmetry points in the BZ, namely, the H point $2\pi/a(1,0,0)$, where a is the lattice constant, and the N point $\pi/a(1,1,0)$. For the H-point phonons, the longitudi-

nal and transverse modes are degenerate due to symmetry, but not for the N-point phonons whose transverse modes we denote as T_1 and T_2 and longitudinal mode as L. Hence, we have considered four phonon modes as a function of pressure up to 10 Mbar. Four different displacements, inducing not more than $2-3$ mRy shift in the total energy, were typically used to fit Eq. (1). Details on how these displacements were chosen are given in Appendix A together with the respective Bravais lattices we have used for the H and N phonons. The number of k points for these 2-atom/cell calculations were about $600-900$ in the irreducible part of the BZ, depending on the actual phonon mode.

III. EQUATION OF STATE

In this section we present a detailed analysis of the pressure versus volume or zero-temperature equation of state (EOS) of bcc Ta, including both our central FP-LMTO result and its sensitivity to various approximations. The results discussed have been obtained from the ''local-fit'' scheme described in the previous section. However, it may be of interest to some readers to see our central EOS result represented by a global Murnaghan fit as well. The global Murnaghan expression for the total energy can be written as

$$E_{\text{tot}}(V) = \left(\frac{B_0 V}{B_0'} \right) \left[\frac{1}{B_0'} \left(\frac{V_0}{V} \right)^{B_0'} + 1 \right] + E_0. \tag{2}$$

The four fitting parameters correspond to measurable quantities: B_0 and B_0' are the bulk modulus and its pressure derivative, respectively, V_0 is the equilibrium volume and E_0 is an additive constant related to the cohesive energy. For Ta our global least-squares fit gives $V_0 = 17.70$ Å^3, $B_0 = 2.18$ Mbar, and $B_0' = 3.2$. These values are similar but not identical to those obtained from the ''local-fit'' scheme: $V_0 = 17.68$ Å^3, $B_0 = 2.03$ Mbar, and $B_0' = 4.3$. This reflects the limitations of the Murnaghan functional form when applied to such a large pressure range. Other global EOS schemes may or may not do better. We find, for example, that the universal-equation-of-state (UEOS) scheme of Vinet et $al.$,[24] which similarly employs V_0, B_0, and B_0' as parameters, only gives an accurate fit to the present Ta EOS to about 2 Mbar. However, a modified UEOS scheme[25] with three additional parameters (corresponding to higher pressure derivatives) does adequately describe the Ta EOS over the entire $0-10$ Mbar range and with parameter values close to those of our ''local-fit'' scheme: $V_0 = 17.68$ Å^3, $B_0 = 2.07$ Mbar, and $B_0' = 4.4$.

In order to perform sensitivity tests and to compare with previous theoretical results for the equation of state for Ta, we have considered the effects of common approximations that have been widely used for electronic structure calculations. Specifically, we have considered an LDA approach to the exchange-correlation functional suggested by von Barth and Hedin[26] in addition to the GGA proposed by Perdew and co-workers.[18] We also have switched on and off the spin-orbit (SO) interaction in our calculations, with the no spin-orbit case (NSO) corresponding to the familiar semi- or scalar-relativistic approximation. In Fig. 1 we compare our calculated EOSs of Ta up to 1 Mbar for the four possible combinations of these two approximations with experimental diamond-anvil-cell (DAC) data[5] taken at room temperature.
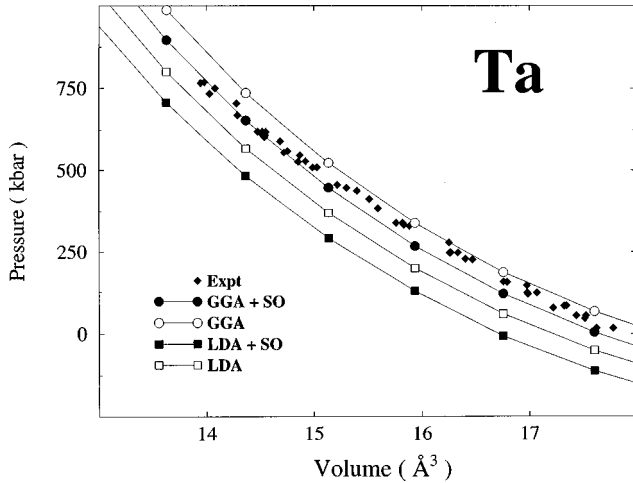
FIG. 1. Theoretical (FP-LMTO) and experimental (DAC) equations of state for Ta below 1 Mbar. Theory including gradient corrections and spin-orbit coupling (GGA + SO, see main text) gives an equilibrium volume (17.68 Å^3) closest to experiment (17.88 Å^3).

Note that the calculation that in principle should be the most accurate, i.e., the GGA + SO result with a gradient-corrected exchange-correlation functional and with the spin-orbit interaction included, reproduces the experimental data most accurately overall. This calculation also reproduces the estimated experimental zero-temperature equilibrium volume[27] to within about 1%, as shown in Table I. Interestingly, the LDA without spin-orbit coupling also gives a reasonably good overall description here and definitely better results than the LDA with spin-orbit coupling, which underestimates the zero-temperature equilibrium volume significantly for Ta, as also shown in Table I. Clearly, the scalar relativistic treatment compensates for errors in the LDA to some extent. These results suggest that unless an electronic-structure calculation for Ta includes a gradient-corrected exchange-correlation functional, it is probably not a good idea to include spin-orbit coupling. Finally, it is also reassuring to note from Table I that the LDA calculation performed by Wu et al.[28] without spin-orbit coupling, using an independent FP-LMTO method,[29] gives a very similar equilibrium volume for Ta (17.33 Å^3) compared to our corresponding LDA-NSO calculation (17.25 Å^3).

In addition to the two aforementioned approximations, the so-called atomic sphere approximation (ASA), where a spherically symmetric potential and charge density is assumed in addition to other approximations,[30] has been widely used to calculate equations of state for many metals. For this reason we also have performed LMTO-ASA calculations of the equilibrium volume for Ta as a further point of reference. These calculations also can be either scalar relativistic (Pauli Hamiltonian with relativistic terms except spin-orbit coupling) or fully relativistic (Dirac Hamiltonian with relativistic terms including the spin-orbit coupling). The results of these calculations are shown in Table I and they indicate larger equilibrium volumes of 18.7 Å^3 (scalar relativistic) and 18.6 Å^3 (fully relativistic). Here we have again used the von Barth and Hedin exchange-correlation functional.[26] It has been shown previously that gradient corrections to that functional worsen the results for methods that neglect nonspherical charge density[31] and for that reason we did not perform LMTO-ASA calculations with the GGA. Although Ta is not an especially favorable case, the combination of the ASA and the LDA is often a good one for equation-of-state calculations, since these approximations have a consistent, but opposite effect upon the calculated equilibrium volume of a metal. The LDA overestimates chemical bonding while the ASA underestimates this bonding, leading to a cancelation of errors with a relatively small net effect on the calculated equilibrium volume. It has been noted[32] that the ASA tends to increase the calculated equilibrium volumes, often concealing the disagreement of the full-potential LDA with experiment. One should remember, however, that the total energies calculated for open crystal structures or used to obtain elastic constants and frozen phonons are not sufficiently accurate with the ASA.

It is also interesting to note in Table I that the spin-orbit interaction has a larger effect on decreasing the equilibrium volume for LMTO calculations done with the full potential as compared to calculations performed within the ASA. We speculate that the semicore states, defined in our FP-LMTO calculations but not in the LMTO-ASA calculations, are more sensitive to the spin-orbit splitting leading to an increase in the chemical bonding. Similar observations have been made for the actinide metals, where spin-orbit coupling increases the atomic volume when the semi-core states are neglected. When they are included, however, the net effect of the spin-orbit interaction has on the equilibrium volume is small for metals such as Pu.

TABLE I. Calculated equilibrium volumes V_{theory} (in Å^3) for Ta obtained from LMTO calculations in various approximations. Estimated zero-temperature experimental volume V_{expt} is 17.88 Å^3.

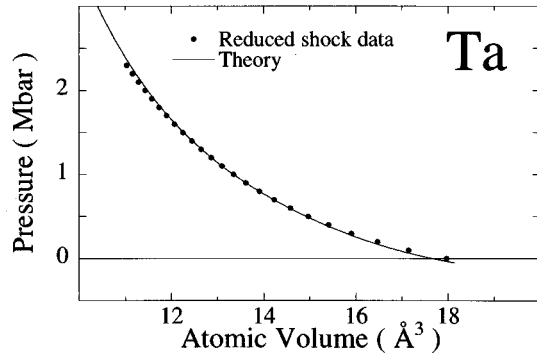| Method	Exchange-correlation	Spin-orbit coupling	V_{theory}	$\dfrac{V_{theory} - V_{expt}}{V_{expt}}$
FP-LMTO	GGA	YES	17.68	−1.1%
FP-LMTO	LDA	YES	16.76	−6.3%
FP-LMTO	GGA	NO	18.21	1.8%
FP-LMTO	LDA	NO	17.25	−3.5%
FP-LMTO [a]	LDA	NO	17.33	−3.1%
LMTO-ASA	LDA	YES	18.60	4.0%
LMTO-ASA	LDA	NO	18.70	4.6%

[a]Wu et al. (Ref. 28).

FIG. 2. Preferred theoretical zero-temperature equation of state (FP-LMTO-GGA-SO) compared against that derived from experimental shock-wave measurements (Ref. 1).

It is encouraging to note that of all the above calculations, the preferred and most accurate theoretical treatment (FP-LMTO-GGA-SO, with spin-orbit coupling included) indeed is reproducing the experimental data best for the equation of state and equilibrium volume of Ta. To test the accuracy of this treatment at somewhat higher pressures, we have compared our calculated EOS with the shock-derived zero-temperature isotherm of McQueen *et al.*,[1] which extends to 2.3 Mbar. This comparison is shown in Fig. 2. The agreement is clearly excellent.

IV. CRYSTAL STRUCTURE STABILITIES

Using our preferred FP-LMTO-GGA-SO theoretical treatment, we have studied the stability of four crystal structures in Ta over the $0-10$ Mbar pressure range. In addition to the observed bcc structure, we have considered the close-packed fcc and hcp structures and also the low-symmetry $A15$ structure. The latter structure occurs frequently in group-V and -VI transition-metal binary compounds, and there also has been recent experimental evidence in Ta that the $A15$ phase can be solidified from the supercooled liquid.[33] Corresponding first-principles calculations[33] have confirmed that the total energy of the $A15$ phase in Ta is close to that of the bcc phase at the equilibrium volume. In Fig. 3, we show the results from our total-energy calculations. Here we plot the
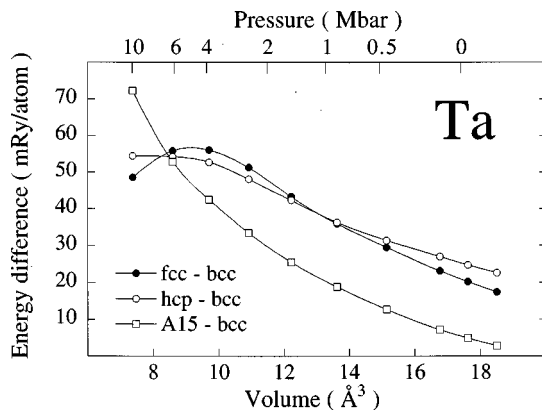
TABLE II. Theoretical structural energies (FP-LMTO-GGA-SO) for Ta under compression. Volumes are in a.u., pressures in Mbar, and energy differences in mRy/atom. For conversion of volumes to Å^3 units, $V(\text{Å}^3) = 0.14818\, V(\text{a.u.})$.

Volume	Pressure	fcc$-$bcc	hcp$-$bcc	$A15-$bcc
124.8	-0.08	17.4	22.6	2.8
118.9	0.005	20.2	24.7	4.9
113.1	0.12	23.1	27.0	7.2
102.2	0.45	29.5	31.4	12.7
91.95	0.90	35.9	36.3	18.8
82.45	1.53	43.3	42.3	25.5
73.62	2.48	51.3	48.1	33.5
65.44	3.89	56.1	52.8	42.5
57.91	6.00	55.9	54.3	52.9
49.65	10.0	48.6	54.5	72.3

energies of the fcc, hcp, and $A15$ structures relative to that of the bcc ground-state as a function of volume. Corresponding numerical values are given in Table II. In these calculations, we have kept the c/a axial ratio in the hcp structure at the ideal value, since optimizing this ratio would lower the hcp energy only slightly. This was directly verified for one volume (102.2 a.u. $=$ 15.14 Å^3), where the optimized c/a ratio was calculated to be about 1.80, with a corresponding lowering of the hcp energy by about 4 mRy/atom. At this volume, the minimum hcp energy is still about 27 mRy higher than the bcc energy (see Table II). Also note in Fig. 3 that the $A15$ structure is indeed very close in energy to the bcc structure at low pressures, whereas both the fcc and hcp structures lie much higher in energy. The trend suggests that at slightly more expanded conditions the $A15-$bcc energy difference would, in fact, pass through zero. Extrapolating from Table II, we find that this should occur at a volume of about 132.7 a.u. (19.66 Å^3), which is very close to the observed solid volume of 133.2 a.u. (19.74 Å^3) for the bcc phase at melt.[34] With increasing pressure, on the other hand, the bcc structure becomes rapidly more stable with respect to the other three structures. At high pressures above 4 Mbar, however, the hcp$-$fcc energy difference levels off and becomes nearly constant, while the fcc$-$bcc energy difference maximizes and then begins to slowly decline.
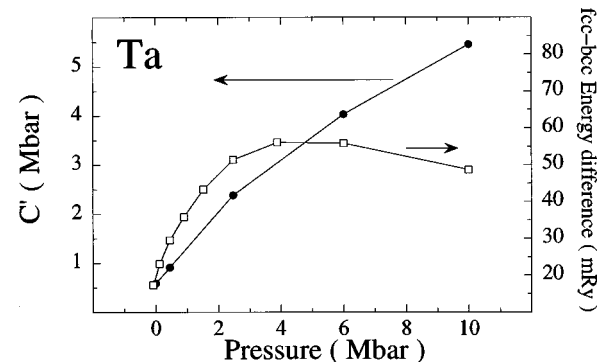
The large energy difference between the bcc and fcc

FIG. 3. Total energies in Ta as a function of volume for the ideal hcp, fcc, and $A15$ structures relative to the observed bcc structure. On top of the figure the bcc pressure, as obtained from the present Ta EOS, is shown.

FIG. 4. Tetragonal shear constant C' and fcc$-$bcc crystal-structure energy difference for Ta as a function of pressure, as obtained from the Ta EOS.
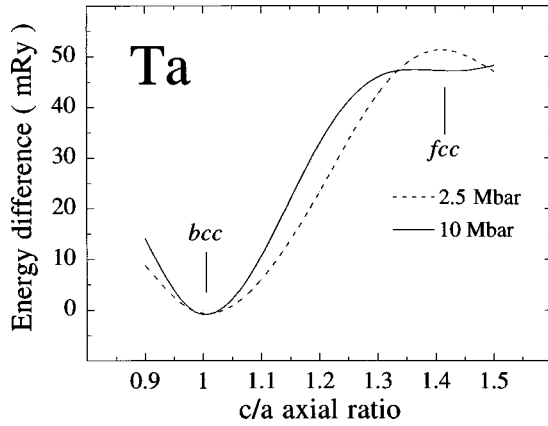
FIG. 5. Calculated total energy for bct Ta at 2.5 and 10 Mbar as a function of c/a axial ratio (the Bain transformation path). The high symmetry values $c/a = 1$ and $c/a = \sqrt{2}$ correspond to the bcc and fcc crystal structures, respectively.

structures is typical for a metal with a high tetragonal shear constant C'. In fact, it has been previously demonstrated that these two properties scale fairly well for most d-transition metals.[35] Although the bulk modulus shows a parabolic variation with atomic number as one proceeds through the $4d$ or $5d$ transition series, with a maximum in the middle of the series, the variation of C' is not parabolic. Instead the fcc−bcc energy difference is the most important controlling factor and this energy difference is determined primarily by the d-band energy. However, the scaling principle between the fcc−bcc energy difference and C' noted at ambient conditions has not been tested heretofore as a function of pressure. In Fig. 4 we plot both these quantities for Ta up to 10 Mbar. The fcc−bcc energy difference is increasing with pressure and up to about 4 Mbar the scaling principles holds fairly well. At higher pressures where the fcc−bcc energy difference maximizes and then begins to decrease, the tetragonal shear constant continues to increase with pressure in a nearly linear fashion. This peculiar behavior can be traced to the shape of the so-called Bain transformation path. This path defines the total energy as a function of tetragonal distortion of a bct unit cell where the distortion parameter is the c/a axial ratio. For the values $c/a = 1$ and $c/a = \sqrt{2}$ we recover the bcc and the fcc crystal structures, respectively. The curvature of this path at $c/a = 1$ gives the bcc tetragonal elastic constant C'. The curvature (and therefore C') is of course related to the fcc−bcc energy difference, and if this path has the general shape shown for Ta at 2.5 Mbar in Fig. 5, then C' and the fcc−bcc energy difference are found to

be roughly proportional. However, at higher pressure (~ 10 Mbar) in Ta the Bain path becomes distorted near the fcc end, so that the curvatures at $c/a = 1$ and $c/a = \sqrt{2}$ have completely different magnitudes. In fact, the fcc structure at this pressure has a small but *positive* curvature indicating a positive fcc C'. For all d-transition metals at ambient pressure[36] and also for Ta up to about 2–3 Mbar, the Bain path has a symmetric shape where the curvature is very similar in magnitude for $c/a = 1$ (bcc) and $c/a = \sqrt{2}$ (fcc) but with different signs. For Ta at ultrahigh pressure, this general form of the Bain path is altered as the fcc C' changes sign from negative to positive. The underlying reason for this change in behavior appears to be related to the fact that the electrostatic contribution to the total energy becomes increasingly more important at ultrahigh pressure and this contribution works to stabilize high-symmetry closed-packed structures such as fcc. At lower pressures, on the other hand, the band-structure energy and its difference as a function of crystal structure is more important. In fact, it has been shown that band-filling effects can explain the behavior of the fcc−bcc energy difference and also C' for d-transition metals and their alloys.[37] Since the fcc C' becomes positive at about 10 Mbar in Ta, we also considered an orthorhombic (or trigonal) distortion of the fcc structure corresponding to the other shear elastic constant C_{44}. We have found that this distortion also increases the total energy, so that C_{44} is positive as well. Hence, mechanical stability is developed for fcc Ta at ultrahigh pressure. Coupled with the decreasing magnitude of the fcc−bcc energy difference in this pressure regime, this suggests that the fcc phase may eventually become stable over the bcc phase at still higher pressures.

A scenario in which Ta transforms to the fcc structure at some ultrahigh pressure is interesting since this metal is clearly very stable in the bcc phase over a very large pressure range, at least $0 - 10$ Mbar, and elementary arguments based on the expected d-band filling and $sp \rightarrow d$ electron transfer[38] suggest that bcc should remain the ultimate high-pressure phase. However, it has been predicted by Ahuja *et al.*[39] that d-transition metals with a d band occupation between 2 and 5 electrons per atom could be stabilized in the fcc structure if the hybridization between semicore $5p$ and valence $5d$ states is strong enough at high pressure. Tantalum has about 3.4 $5d$ electrons per atom at the equilibrium volume and this occupation is increasing with pressure via $sp \rightarrow d$ electron transfer due to broadening of the bands and the relative lowering of the $5d$ bands compared to the $6s$ and $6p$ bands. Hence, Ta is lying in the $2 - 5$ d-electron range for which the fcc structure would be stabilized due to $5p$-$5d$ hybridization.

TABLE III. Theoretical moduli and phonons (FP-LMTO-GGA-SO) for bcc Ta under compression. Volumes are in a.u., pressures, bulk and elastic moduli in Mbar, and zone-boundary phonons in THz. For conversion of volumes to Å^3 units, $V(\text{Å}^3) = 0.14818\, V(\text{a.u.})$.

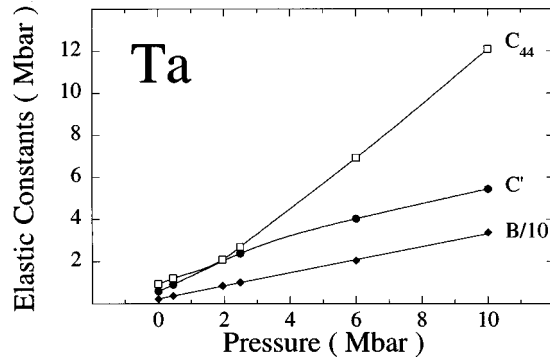| Volume	Pressure	B	C'	C_{44}	L	T_1	T_2	H
118.9	0.005	2.03	0.59	0.93	4.79	2.68	4.52	5.49
102.2	0.45	3.70	0.91	1.20	6.78	3.36	5.02	6.96
73.62	2.48	10.1	2.38	2.69	12.0	5.45	6.40	10.2
57.91	6.00	20.4	4.03	6.92	15.6	6.71	8.24	13.2
49.65	10.0	33.8	5.45	12.1	17.2	8.0	9.66	16.0

FIG. 6. Bulk modulus B and shear elastic constants C' and C_{44} as a function of pressure for bcc Ta.

It is clear from Fig. 3, however, that the pressure required for this transition (bcc → fcc) is well above our highest studied pressure, 10 Mbar.

V. ELASTIC CONSTANTS AND PHONONS

In this section we report our calculated results for the elastic constants and high-symmetry zone-boundary phonons of bcc Ta. Here we have again used our preferred FP-LMTO-GGA-SO treatment, which gives the most accurate results for the equation of state. The calculation of the shear elastic constants involves computing the change in total energy for appropriate small applied strains and the specific procedure developed for cubic metals has been detailed in a previous paper.[37] Our results for these quantities, as well as the bulk modulus obtained from the zero-temperature EOS, are given in Table III and Fig. 6 over the $0-10$ Mbar pressure range. The bulk modulus B and the shear elastic moduli C' and C_{44} are everywhere calculated to be positive and show smooth monotonic behavior as a function of pressure. This indicates full mechanical stability for bcc Ta over the entire $0-10$ Mbar pressure range. Note that in Fig. 6 we have scaled B by a factor of 10 so that its magnitude becomes more similar to C' and C_{44}. At ambient pressure, our calculated bulk and shear moduli are in good agreement with ultrasonic measurements,[8] as shown in Table IV. Under compression, C_{44} increases more rapidly with pressure than C'. This indicates that Ta is increasingly anisotropic at high pressure, and the anisotropy ratio

$$A = C_{44}/C' \qquad (3)$$

increases from 1.58 at ambient pressure to a value of 2.22 at 10 Mbar. Although such an increase is somewhat counterin-
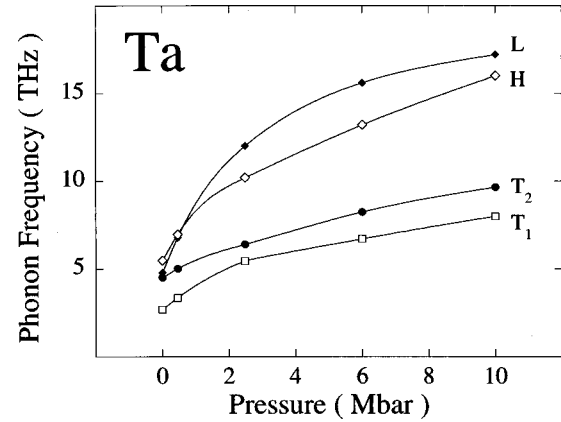

FIG. 7. High-symmetry H, L, T_1, and T_2 zone-boundary phonons (see text) for bcc Ta as a function of pressure.

tuitive, it is not uncommon in metals. For example, we have found qualitatively similar behavior in high-pressure iron.[20] Experiments to measure the high-pressure elastic constants of Ta are currently in progress.[13]

In addition to the elastic constants, we have also studied the H- and N-point zone-boundary phonons in bcc Ta up to 10 Mbar, by means of the frozen-phonon method (see Sec. II and the Appendix), and the results are given in Table III and Fig. 7. Note from the figure that at low pressure the frequencies of the H-point phonon and the longitudinal mode L of the N-point phonons are rising rapidly and cross at about 0.5 Mbar, but above about 2 Mbar all of the calculated phonons show a very similar (almost linear) pressure dependence. At ambient pressure, our calculated results are in good agreement with those obtained from room-temperature inelastic neutron scattering measurements,[40] as shown in Table IV. The N-point phonons for Ta at the equilibrium volume were also recently calculated using an *ab initio* pseudopotential method (PP-LDA-NSO) by Wu *et al.*,[28] and as shown in the same table, these results agree favorably with ours. An interesting aspect of the experimental data is the accidental degeneracy found for the L and T_2 phonons. The qualitative origin of this degeneracy can be seen from Fig. 7, where the frequency of the L mode is seen to be rapidly approaching that of the T_2 mode near zero pressure. In our calculation at zero pressure, however, the L and T_2 frequencies differ by about 5% and in the calculation of Wu *et al.*[28] by about 12%. This outcome partly reflects the sensitivity of the L mode to volume at low pressure. If we extrapolate our results from the calculated zero-temperature equilibrium volume of 118.9 a.u. to the observed room-temperature equilibrium volume of

TABLE IV. Theoretical and experimental ambient-pressure bulk and shear elastic moduli (in Mbar) and zone-boundary phonons (in THz) for bcc Ta.

Treatment	B	C'	C_{44}	L	T_1	T_2	H
PP-LDA-NSO [a]	2.11			4.72	2.74	4.17	
FP-LMTO-LDA-NSO [a]	1.98						
FP-LMTO-GGA-SO	2.03	0.59	0.93	4.79	2.68	4.52	5.49
Experiment [b]	1.96	0.525	0.825	4.35±0.08	2.63±0.08	4.35±0.06	5.03±0.07

[a]Wu *et al.* (Ref. 28).
[b]Moduli from Katahara *et al.* (Ref. 8) and phonons from Woods (Ref. 40).

121.6 a.u., the L phonon frequency is reduced to about 4.54 THz and the observed accidental degeneracy between L and T_2 is nearly achieved.

VI. SHEAR STRENGTH

In this section we first use our calculated bcc elastic constants to analyze the assumed pressure dependence of the well known Steinberg-Guinan (SG) strength model[10] as applied to polycrystalline Ta and then discuss our calculation of the ideal strength of the bcc metal. This will allow us to put approximate lower and upper bounds on the high-pressure yield strength of Ta.

The phenomenological SG strength model assumes that the yield stress of a metal scales linearly with its average shear modulus G in the form

$$Y = Y_0 f(\epsilon_p) G(P,T)/G_0, \qquad (4)$$

where Y_0 is a constant (1.63 GPa = 0.0163 Mbar for Ta) and f is a bounded function of plastic strain ϵ_p, such that

$$1 \leq f(\epsilon_p) \leq Y_{max}/Y_0, \qquad (5)$$

with Y_{max} a second constant (1.93 GPa for Ta). In addition, simple assumptions are made about how the shear modulus G varies with pressure P and temperature T. The temperature dependence of G is modest compared to its pressure dependence, so we focus only on the latter. At $T = 300$ K, it is assumed that

$$G(P,300) = G_0(1 + A_0 P/\eta^{1/3}), \qquad (6)$$

where

$$A_0 = \frac{1}{G_0}\frac{dG_0}{dP}, \qquad (7)$$

η is the compression factor V_0/V, and the subscript zero denotes $P=0$. The constants G_0 and A_0 are determined from the measured values of the shear modulus and its first derivative at ambient conditions. Apart from the $\eta^{1/3}$ term, Eq. (6) is a first-order Taylor series expansion in the pressure. The additional term is suggested from Thomas-Fermi theory in the high compression limit[41] and serves to bound G at high pressure.

To compare our first-principles results with Eq. (6), we define a single shear modulus for the metal as the simple Voigt average of the two bcc shear elastic constants:

$$G_V(P) = [2C'(P) + 3C_{44}(P)]/5. \qquad (8)$$

If the ambient-pressure experimental shear-moduli data[8] are inserted into Eq. (8), one infers $G_V(0) = 0.705$ Mbar and $A_V(0) = [G_V(0)]^{-1}dG_V(0)/dP = 1.45$ (Mbar)$^{-1}$, which are close to the values of $G_0 = 0.69$ Mbar and $A_0 = 1.41$ (Mbar)$^{-1}$ used in the SG model for Ta,[10] so we regard this as an adequate averaging procedure. In Fig. 8 we directly compare $G_V(P)$ with the SG model over the 0–10 Mbar pressure range, using the present *ab initio* FP-LMTO values of C' and C_{44} in Eq. (8) and also the corresponding bcc EOS to evaluate the $\eta^{1/3}$ term in Eq. (6). Overall, the agreement is remarkably good, although above about 6 Mbar the present theory predicts a somewhat faster rise in the shear modulus
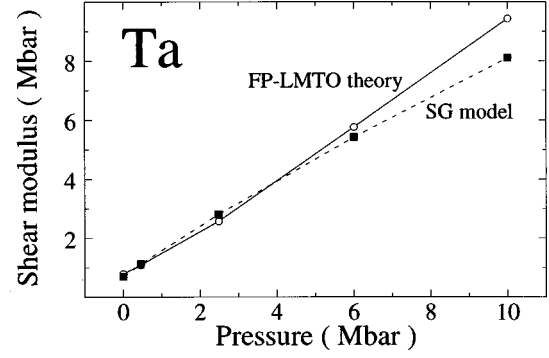

FIG. 8. High-pressure shear modulus for Ta as calculated from the present FP-LMTO elastic moduli via Eq. (8) and from the Steinberg-Guinan model via Eq. (6).

than does the SG model. We make no attempt here to address the adequacy of the SG model itself for the yield stress Y, except to remark that available experimental evidence[10,15] suggests that Y increases faster with pressure than does the shear modulus G. Thus we believe a reasonable lower bound for the high-pressure yield strength is

$$Y_0 G_V(P)/G_V(0), \qquad (9)$$

where Y_0 is taken from the SG model and G_V is taken from theory via Eq. (8).

A corresponding upper bound can be established by considering the ideal theoretical shear strength of the perfect bcc crystal, in the complete absence on any dislocations or grain boundaries. A specific procedure to calculate this quantity for real materials has been suggested and applied to fcc and bcc metals by Paxton *et al.*[42] The ideal shear strength is defined to be the critical stress τ_c separating elastic and plastic deformation under the continuous homogeneous shearing of the perfect crystal into itself via the observed twinning mode. For bcc crystals, this mode is specified by the shear direction $\eta = [\bar{1}\bar{1}1]$ and the normal plane $\mathbf{K} = (112)$. Neglecting any relaxation normal to $\mathbf{K}$, the atomic positions during the deformation can be analytically related to the amount of shear x. Specifically, the calculation may be carried out entirely using a single atom per unit cell and periodic boundary conditions, with the basis vectors of the sheared crystal given by

$$\mathbf{a}_1 = \frac{1}{2}[\bar{1}11] + \frac{1}{6}\frac{x}{s}[\bar{1}\bar{1}1], \qquad (10a)$$

$$\mathbf{a}_2 = \frac{1}{2}[1\bar{1}1] + \frac{1}{6}\frac{x}{s}[\bar{1}\bar{1}1], \qquad (10b)$$

$$\mathbf{a}_3 = \frac{1}{2}[11\bar{1}]. \qquad (10c)$$

At $x = s = 1/\sqrt{2}$, one has $\mathbf{a}_1 = \frac{1}{3}[\bar{2}12]$ and $\mathbf{a}_2 = \frac{1}{3}[1\bar{2}2]$, so that an exact bcc twin has been created. Along the twinning path one calculates a symmetric energy barrier,
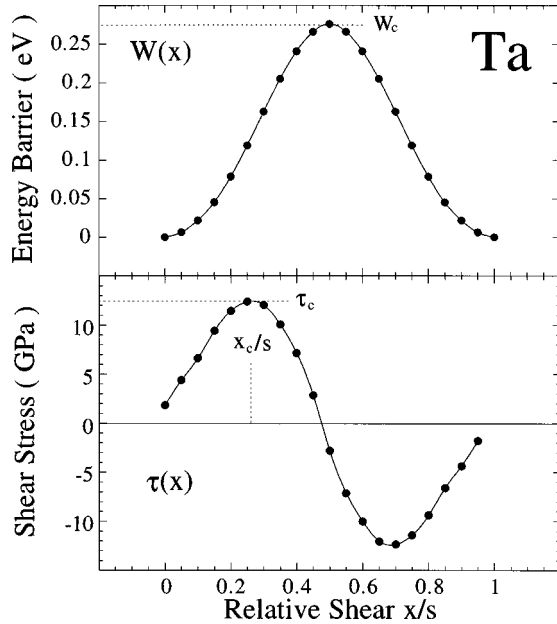
$$W(x) = (E_{tot}[V,x] - E_{tot}[V,0])/N, \qquad (11)$$

FIG. 9. Calculated ideal shear strength in bcc Ta at a volume of 102.2 a.u. Upper panel shows the energy barrier $W(x)$ and the lower panel the shear stress $\tau(x)$.

with a barrier height W_c at $x = s/2$. The corresponding stress is given by

$$\tau(x) = \frac{1}{V} \frac{dW(x)}{dx}. \qquad (12)$$

The ideal shear strength is identified with the maximum calculated stress along the twinning path, $\tau_c = \tau(x_c)$, where x_c is the critical shear separating regimes of elastic and plastic deformation of the crystal. Paxton et al.[42] carried out this procedure for five bcc transition metals at ambient pressure, excluding Ta, using an independent FP-LMTO method. These calculations were non-self-consistent, however, and employed the so-called Harris-Foulkes approximation to obtain the potential, which they claim reproduces a full self-consistent calculation of τ_c in vanadium to within about 5%. This simplification also allowed these authors to consider relaxation effects, but these were found to be small in all cases and did not change τ_c by a significant amount. In the present work, therefore, we have considered only the unrelaxed case.

Our ideal shear strength calculations for Ta have been carried out in a very similar manner to our calculations of the

crystal structure stabilities described in Secs. II and IV. Here we have used Eqs. (10a)–(10c) to define the one-atom/cell crystal structure for which we then perform a total energy calculation. For each volume V considered, we have calculated the total energy for 11 relative shears (x/s) in the interval $0 \leqslant x/s \leqslant 0.5$, noting that the interval $0.5 \leqslant x/s \leqslant 1.0$ can be obtained by symmetry (i.e., x/s and $1 - x/s$ define the same crystal structure). This energy path as a function of x/s was so calculated for five different volumes. For the smaller volumes we used up to about 2000 k points in the irreducible part (1/4th) of the Brillouin zone to safely converge the total energy. Representative results for the resulting energy barrier $W(x)$ and shear stress $\tau(x)$ at a single volume are plotted in Fig. 9. Note in the upper panel of Fig. 9 that our calculated $W(x)$ varies very smoothly with shear x. This allowed us to easily numerically differentiate this energy to obtain the shear stress $\tau(x)$, shown in the lower panel of Fig. 9.

Calculated values of the barrier height W_c, critical stress τ_c, critical shear x_c, and the shear modulus in the $\langle 111 \rangle$ direction

$$G_{111} = (2C' + C_{44})/3 \qquad (13)$$

are listed in Table V. The barrier height and critical stress display the expected monotonic increase with increasing pressure and decreasing volume. The relative critical shear x_c/s remains in the approximate range $0.26 - 0.28$ and close to the value 0.25 one would have if $\tau(x)$ were a pure sine function, as in the elementary Frenkel model of ideal strength.[43] The relative critical stress τ_c/G_{111} remains in the approximate range $0.10 - 0.15$, which is consistent with both the Frenkel model and the $0.12 - 0.17$ range of values found by Paxton et al.[42] for the other bcc transition metals at ambient pressure.

The upper bound to the high-pressure yield strength can simply be taken as $\tau_c(P)$ and compared with the lower bound defined in Eq. (9). In Fig. 10 we plot both $\tau_c(P)$ and $Y_0 G_V(P)/G_V(0)$ as a function of pressure over the $0 - 10$ Mbar range. The striking feature of this result is that the two bounds are not widely separated and differ only by a factor of 4–7 over the whole pressure range. Diamond-anvil-cell experiments to measure the high-pressure yield strength of Ta are currently in progress.[15]

VII. CONCLUSIONS

In this work we have used what we believe is the most accurate version of density-functional theory currently available to predict a number of important high-pressure, zero-

TABLE V. Calculated ideal shear strength parameters for bcc Ta: barrier height W_c in eV, critical shear x_c, critical stress τ_c, and shear modulus G_{111} in GPa. For conversion of volumes to Å^3 units, $V(\text{Å}^3) = 0.14818 \, V(\text{a.u.})$. Note 100 GPa = 1 Mbar.

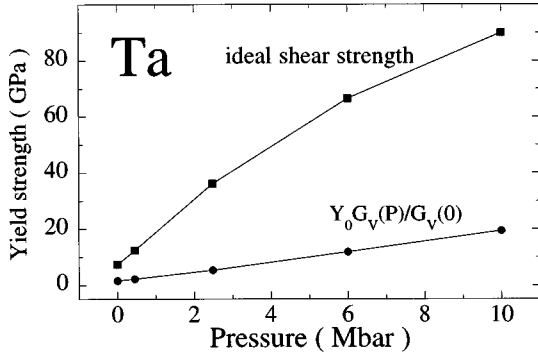| Volume	W_c	x_c/s	τ_c	G_{111}	τ_c/G_{111}
118.9	0.194	0.258	7.37	70.3	0.105
102.2	0.276	0.265	12.4	101	0.123
73.62	0.566	0.280	36.2	248	0.146
57.91	0.837	0.274	66.5	499	0.133
49.65	0.952	0.260	89.9	767	0.117

FIG. 10. Approximate upper and lower bounds on the yield strength of Ta as a function of pressure, as discussed in the text.

temperature properties of Ta up to 10 Mbar. Our fully relativistic FP-LMTO method with GGA exchange and correlation yields a quantitatively accurate equilibrium volume and equation of state for this metal and could serve as the basis for developing a more global finite-temperature EOS in the future. We have further shown that the observed bcc structure in Ta should remain both thermodynamically and mechanically stable over the entire $0-10$ Mbar range considered, but that a bcc $\rightarrow$ fcc phase transition is possible at ultrahigh pressure well above 10 Mbar. In the stable bcc phase, both the elastic moduli and high-symmetry zone-boundary phonons display smooth monotonic behavior with pressure, but increasing elastic anisotropy is predicted and this could have important consequences for the high-pressure mechanical properties of Ta. The calculated elastic moduli have also served to confirm the assumed pressure dependence of the shear modulus in the phenomenological Steinberg-Guinan strength model for Ta and in conjunction with that model provide an approximate lower bound on the expected high-pressure yield strength of this metal. Calculations of the ideal shear strength of the perfect bcc metal reveal Frenkel-like behavior and provide a corresponding approximate upper bound to the high-pressure yield strength. These bounds are reasonably closely spaced and should serve as a useful guide to future experimental and theoretical investigations.

Our *ab initio* FP-LMTO results should also be useful in developing corresponding many-body, angular-force interatomic potentials for Ta via model generalized pseudopotential theory[44] (MGPT), as has been done previously for iron[20] and molybdenum (Mo).[44] We envisage that such MGPT potentials will be able to provide the ion-thermal components of thermodynamic properties over $0-10$ Mbar pressure range, including the finite temperature bcc EOS, melting, and the EOS of the molten liquid metal. We further intend to extend the FP-LMTO calculations to finite temperature to treat the corresponding electron-thermal components of such properties, which can be quite significant in the central bcc transition metals.[44] With regard to mechanical properties, we expect to be able to use the same MGPT potentials to study relevant point and extended defects in Ta, including the structure and energetics of dislocations, as we have done successfully for Mo.[45] We envisage that such calculations could form the required atomistic basis for a rigorous multiscale treatment of the yield stress and plastic flow in Ta. Finally, it may also be possible to address a few of the sim-

pler defect problems with our *ab initio* FP-LMTO method as well. In this regard, we are currently engaged in preliminary FP-LMTO calculations of the vacancy formation energy.

APPENDIX

In this appendix, we give details regarding the Bravais lattices we have used for our bcc frozen phonon calculations and also the displacements applied. We have studied the H and N points in the Brillouin zone because for these high symmetry zone-boundary phonons it suffices to study a doubled unit cell. For the Bravais lattice of the H phonon we have used the simple cubic unit cell

$$\mathbf{R} = \begin{pmatrix} 1 & 0 & 0 \\ 0 & 1 & 0 \\ 0 & 0 & 1 \end{pmatrix}. \qquad (A1)$$

For the N phonon we instead have used the Bravais lattice defined by

$$\mathbf{R} = \begin{pmatrix} -\frac{1}{2} & \frac{1}{2} & \frac{1}{2} \\ \frac{1}{2} & -\frac{1}{2} & \frac{1}{2} \\ 1 & 1 & 0 \end{pmatrix}. \qquad (A2)$$

These Bravais lattices are here given in units of the lattice constant a. The doubled cell for both the H and N phonons have atoms in equilibrium positions $(0,0,0)$ and $(\frac{1}{2},\frac{1}{2},\frac{1}{2})$. (Atomic positions are here represented in their respective Bravais lattice coordinates.) In the frozen-phonon method the energy increase (ΔE) associated with a phonon displacement, $u_{\mathbf{q}} = u|\mathbf{q}|a$ defined by the normalized wave vector $\mathbf{q}$, is calculated and the corresponding angular frequency can be obtained by means of Eq. (1). In general, one can use the following displacements of the atoms: for the H-point phonon $(0,0,u)$ and $(\frac{1}{2},\frac{1}{2},\frac{1}{2}-u)$; for the two transverse modes of the N point phonon $(-u,u,0)$ and $(\frac{1}{2}+u,\frac{1}{2}-u,\frac{1}{2})$ for T_1 and $(u,u,0)$ and $(\frac{1}{2}-u,\frac{1}{2}-u,\frac{1}{2})$ for T_2; and for the longitudinal N-point phonon $(0,0,u)$ and $(\frac{1}{2},\frac{1}{2},\frac{1}{2}-u)$. In practice, we let one of the atoms be fixed and displace the other by the relative displacement between the two, e.g., $(\frac{1}{2},\frac{1}{2},\frac{1}{2}-2u)$ for the H-point phonon. By calculating total energies and extracting ΔE, the angular frequency can be obtained from the harmonic relation

$$\omega_{\mathbf{q}} = \sqrt{\frac{2\Delta E}{Mu^2|\mathbf{q}|^2 a^2}}. \qquad (A3)$$

[1] R.G. McQueen, S.P. Marsh, J.W. Taylor, J.M. Fritz, and W.J. Carter, in *High Velocity Impact Phenomena*, edited by R. Kinslow (Academic, New York, 1970), p. 293.

[2] A.C. Mitchell and W.J. Nellis, J. Appl. Phys. **52**, 3363 (1981).

[3] L.V. Al'tshuler, A.A. Bakanova, I.P. Dudoladov, E.A. Dynin, R.F. Trunin, and B.S. Chekin, Sov. J. Appl. Mech. Tech. Phys. **22**, 145 (1981); K.K. Krupnikov, A.A. Bakanova, M.I. Brazknik, and R.F. Trunin, Sov. Phys. Dokl. **8**, 205 (1963).

[4] L.-C. Ming and M.H. Manghnani, J. Appl. Phys. **49**, 208 (1978).

[5] J. Xu, H.-K. Mao, and P.M. Bell, High Temp.-High Press. **16**, 495 (1984).

[6] H.K. Hoge and A.K. Mukherjee, J. Mater. Sci. **12**, 1666 (1977).

[7] L.P. Kubin, Rev. Deform. Behav. Mater. **1**, 244 (1977), and references therein.

[8] K.W. Katahara, M.H. Manghnani, and E.S. Fisher, J. Phys. F **9**, 773 (1979).

[9] D.J. Steinberg and C.M. Lund, J. Appl. Phys. **65**, 1528 (1989), and references therein.

[10] D.J. Steinberg, S.G. Cochran, and M.W. Guinan, J. Appl. Phys. **51**, 1498 (1980), and references therein.

[11] See, for example, *Journal of Computer-Aided Materials Design, Proceedings of the Workshop on Modeling Industrial Materials: Connecting Atomistic and Continuum Scales*, edited by S. Yip (ESCOM, Leiden, 1996), Vol. 3.

[12] A.K. Singh, H.-K. Mao, J. Shu, and R.J. Hemley, Phys. Rev. Lett. **80**, 2157 (1998).

[13] C.-S. Yoo (private communication).

[14] R.J. Hemley, H.-K. Mao, G. Shen, J. Badro, P. Gillet, M. Hanfland, and D. Häusermann, Science **276**, 1242 (1997).

[15] S. Weir (private communication).

[16] P. Hohenberg and W. Kohn, Phys. Rev. **136**, B864 (1964).

[17] W. Kohn and L.J. Sham, Phys. Rev. **140**, A1133 (1965).

[18] J.P. Perdew, J.A. Chevary, S.H. Vosko, K.A. Jackson, M.R. Pederson, D.J. Singh, and C. Fiolhais, Phys. Rev. B **46**, 6671 (1992).

[19] J.M. Wills (unpublished); P. Söderlind, Ph.D. thesis, Uppsala University, 1994; J. Trygg, Ph.D. thesis, Uppsala University, 1995.

[20] P. Söderlind, J.A. Moriarty, and J.M. Wills, Phys. Rev. B **53**, 14 063 (1996).

[21] F.D. Murnaghan, Proc. Natl. Acad. Sci. USA **30**, 244 (1944).

[22] J.A. Moriarty, Phys. Rev. B **8**, 1338 (1973).

[23] K.-M. Ho, C.L. Fu, B.N. Harmon, W. Weber, and D.R. Hamann, Phys. Rev. Lett. **49**, 673 (1982).

[24] P. Vinet, J.H. Rose, J. Ferrante, and J.R. Smith, J. Phys.: Condens. Matter **1**, 1941 (1989); P. Vinet, J. Ferrante, J.H. Rose, and J.R. Smith, J. Geophys. Res. **92**, 9319 (1987).

[25] J.A. Moriarty, High Press. Res. **13**, 343 (1995).

[26] U. von Barth and L. Hedin, J. Phys. C **5**, 1629 (1972); J.F. Janak, V.L. Moruzzi, and A.R. Williams, Phys. Rev. B **12**, 1257 (1975).

[27] B. Eisenmann and H. Schäfer, in *Structure Data of Elements and Intermetallic Phases*, edited by K.-H. Hellwege and A.M. Hellwege, Landolt-Börnstein, New Series, Group III, Vol. 14, Pt. a (Springer-Verlag, Berlin, 1988).

[28] C.J. Wu, L.H. Yang, J.E. Klepeis, and C. Mailhiot, Phys. Rev. B **52**, 11 784 (1995).

[29] M. Methfessel, Phys. Rev. B **38**, 1537 (1988).

[30] H.L. Skriver, *The LMTO Method* (Springer-Verlag, Berlin, 1984).

[31] J. Häglund, Phys. Rev. B **47**, 566 (1993).

[32] K.B. Hathaway, H.J.F. Jansen, and A.J. Freeman, Phys. Rev. B **31**, 7603 (1985).

[33] L. Cortella, B. Vinet, P.J. Desre, A. Pasturel, A.T. Paxton, and M. van Schilfgaarde, Phys. Rev. Lett. **70**, 1469 (1993).

[34] J.W. Shaner, G.R. Gathers, and C. Minichino, High Temp.-High Press. **9**, 331 (1977).

[35] P. Söderlind, R. Ahuja, O. Eriksson, J.M. Wills, and B. Johansson, Phys. Rev. B **50**, 5918 (1994).

[36] J.M. Wills, O. Eriksson, P. Söderlind, and A.M. Boring, Phys. Rev. Lett. **68**, 2802 (1992).

[37] P. Söderlind, O. Eriksson, J.M. Wills, and A.M. Boring, Phys. Rev. B **48**, 5844 (1993).

[38] J.A. Moriarty, Phys. Rev. B **45**, 2004 (1992).

[39] R. Ahuja, P. Söderlind, J. Trygg, J. Melsen, J.M. Wills, B. Johansson, and O. Eriksson, Phys. Rev. B **50**, 14 690 (1994).

[40] A.D.B. Woods, Phys. Rev. **136**, A781 (1964).

[41] M. Guinan and D. Steinberg, J. Phys. Chem. Solids **36**, 829 (1975).

[42] A.T. Paxton, P. Gumbsch, and M. Methfessel, Philos. Mag. Lett. **63**, 267 (1991).

[43] C. Kittel, *Introduction to Solid State Physics*, 5th ed. (Wiley, New York, 1976), p. 565.

[44] J.A. Moriarty, Phys. Rev. B **49**, 12 431 (1994); **42**, 1609 (1990).

[45] W. Xu and J.A. Moriarty, Phys. Rev. B **54**, 6941 (1996); Comput. Mat. Sci. (to be published).